metals

MDPI

Review

Solute Effect on Grain Refinement of Al- and Mg-Alloys: An Overview of the Recent Advances Made by the LiME Research Hub

Feng Gao and Zhongyun Fan *

Brunel Centre for Advanced Solidification Technology (BCAST), Brunel University London, Uxbridge UB8 3PH, UK
* Correspondence: zhongyun.fan@brunel.ac.uk

Abstract: Grain refinement is of importance for metallic materials since it provides multiple benefits, such as improved castability, reduced casting defects and improved mechanical properties. From extensive research carried out in the past decades, it has been widely accepted that solute is one of the crucial factors for achieving grain refinement. However, grain refinement is a complex phenomenon, depending on not only solutes in the melt to provide growth restriction but also the physical and chemical nature of the nucleant particles (either endogenous or exogenous). Although significant progress has been made on the subject, some critical questions still remain open, and a comprehensive understanding of the mechanisms of solute effect on grain refinement is still desirable. In this paper, we present an overview of the solute effect on grain refinement based on our recent advances made in the LiME Research Hub. This covers the effect of solute on nucleation potency of nucleant particles due to interfacial segregation, columnar to equiaxed transition (CET), growth restriction and eventually on the overall grain refinement.

Keywords: grain refinement; nucleation; grain initiation; growth restriction; solute

Citation: Gao, F.; Fan, Z. Solute Effect on Grain Refinement of Al- and Mg-Alloys: An Overview of the Recent Advances Made by the LiME Research Hub. *Metals* **2022**, *12*, 1488. https://doi.org/10.3390/met12091488

Academic Editor: Pavel Lejček

Received: 10 August 2022
Accepted: 5 September 2022
Published: 8 September 2022

1. Introduction

Aluminium (Al) and magnesium (Mg) alloys have extensive applications in both aerospace and automotive industries for lightweighting to reduce greenhouse gas emissions [1,2]. It is desirable to have a fine and uniform grain structure in the as-cast state of Al and Mg alloys since such a grain refined microstructure provides not only enhanced mechanical properties but also an effective mechanism for controlling the cast defects, such as macro-segregation, porosity and coarse second phase particles [3,4].

The solute effect on grain refinement was attended as early as 1949 by Cibula [5] and has been widely investigated in the following decades [6–9]. It has been generally accepted that two crucial factors affect grain refinement: the presence of solutes in the melt and the existence of nucleant particles [10–13]. During diffusion-controlled solidification, the solute elements accumulate/deplete in the liquid adjacent to the solid–liquid interface, slowing down the growth of the solid phase [14], which is referred to as the growth restriction. Meanwhile, the constitutional supercooling (CS) zone [15,16] is created in front of the solid–liquid interface. Based on such facts, two mechanisms for solute effect on grain refinement have been proposed in the literature: (1) solute growth restriction: solute in the liquid ahead of the growing crystals reduces the growth velocity of the initiated crystals and increases the maximum undercooling achievable before recalescence, allowing more particles to be active for grain initiation and thus reducing the grain size [14,17–20]; (2) CS zone formed by segregating elements: the CS generated by a growing grain will trigger further grain initiation on the next most potent particle present ahead of the solid–liquid interface [21,22]. The first mechanism is adopted to numerically predict grain size with varying solute concentrations for isothermal solidification [14,17–20]. The latter mechanism

is applicable for solidification with a temperature gradient, which has also been applied in the numerical prediction of grain size in a near isothermal solidification process [21,22].

Although a great deal of work, both experimental and theoretical, has been carried out to investigate the mechanisms of solute effect on grain refinement, and reasonable agreements have been achieved between experimental observation and simulated results, there still exist open questions on the role of solutes in grain refinement in both scientific understanding and industrial practice. For example, Tarshis et al. [23] proposed a parameter, P (constitutional supercooling parameter), to quantify the solute effect on grain size, and suggested that there appeared to be a good correlation between grain size and P in Ni- and Al-based alloys, which was supported by Spittle et al. [24,25]. However, Greer et al. [17] suggested that grain size was better described as a function of Q (growth restriction factor) rather than P. A number of studies [21,22,26,27] suggested that grain size ($\bar{d}$) was inversely proportional to the growth restriction factor Q, i.e., $\bar{d} \propto 1/Q$. However, Men and Fan [19] revealed that grain size could be simply related to $(1/Q)^{1/3}$, which was validated by Becerra and Pekguleryuz [28], who experimentally found that grain size was related to $1/Q$ in Mg–Zn alloys, but better described as a function of $(1/Q)^{1/3}$ in Mg–In alloys. Xu et al. [29] experimentally compared the relationships between grain size and three parameters (i.e., P, Q and ΔT_s (solidification interval)) in Al alloys and demonstrated that the measured grain size was more closely related to ΔT_s rather than P and Q. In addition, it was also reported that all these relationships between the grain size and solute growth-restriction-related parameters (P, Q and ΔT_s) obtained from Al and Mg alloys were not applicable to Zn alloys [30].

Another issue is the effect of the CS zone on final grain size. For isothermal or near isothermal solidification, the undercooling in the CS zone is smaller than that outside the CS zone. According to the free growth model [17], there may be no grain formed in the CS zone, which is referred to as the nucleation free zone (NFZ) [22] or solute suppressed nucleation zone (SSNZ) [31]. Shu et al. [31] developed a numerical model to predict the grain size of Al alloys and suggested that grain refinement of alloys of high solute content was controlled primarily by SSNZ. However, Du and Li [32] argued that in their numerical model based on the Kampmann–Wagner model [33], the SSNZ effect could be neglected during isothermal solidification.

The grain size is determined by the grain initiation events at the early stage of solidification [20], such as at recalescence for isothermal solidification where the solid fraction is very small, approximately 10^{-4} under industrially relevant solidification conditions. The early stage of solidification as Fan et al. [20] suggested includes the following steps for a typical solidification of melt with potent nucleant particles: prenucleation, heterogeneous nucleation, constrained cap growth, grain initiation, spherical growth, dendritic growth and recalescence. At the early stage of solidification, the grain initiation that is directly related to the formation of grains, and hence to the final grain size, is determined by the nucleation potency of particles and their number density and size distribution [20]. However, depending on heterogeneous nucleation potency, particle number density and size distribution, grain initiation exhibits different manners [20,34,35], i.e., progressive grain initiation (PGI), explosive grain initiation (EGI) and hybrid grain initiation (HGI), which may lead to different grain refining efficiency of nucleant particles. If other conditions are all fixed to be constant, such as composition, particle number density and size distribution, and cooling rate, increasing nucleation undercooling can significantly promote the grain refining efficiency through EGI [20,34,35]. Recently, it has been recognised that the segregation of solute on the surface of the substrate can change the nucleation potency of the substrate by changing the lattice misfit between the substrate and the solid phase [36–44], the surface roughness of nucleant particles [45–48] and chemical potential [49]. Therefore, the solute effect on grain size can be exhibited by altering the heterogeneous nucleation potency of the substrate, the number density of nucleant particles and the growth restriction in the melt.

In this paper, we aim to present an overview of the solute effect on grain refinement of Al and Mg alloys and offer some suggestions for future research directions on this subject. Firstly, we briefly review the solute effect on heterogeneous nucleation of the particle in Section 2 and then present recent advances in the understanding of the effect of solute growth restriction on grain refinement in Section 3 and a discussion and perspective in Section 4. Finally, a summary will be presented in Section 5.

2. Solute Effect on Heterogeneous Nucleation

2.1. Heterogeneous Nucleation

In practical metallic systems, nucleation during solidification is heterogeneous due to the inevitable existence of solid inclusions in metallic melts [50]. So far, heterogeneous nucleation is usually analysed by classical nucleation theory (CNT) [51–54], which considers the balance between the interfacial energy change and the volume-free energy change during the creation of a spherical cap on a substrate and uses contact angle as a measure for the substrate potency. However, the CNT has been frequently challenged by recent research on heterogeneous nucleation, for example, the validity of the capillarity approximation [55], the discovery of stable prenucleation clusters (PNCs) in aqueous solutions [56], the two-step nucleation pathway [57], barrier-less nucleation of 1D crystals [58] and observation of nucleation in 4D [59].

Both the experimental findings [60,61] and atomistic simulations [62–64] have confirmed that there exists a prenucleation prior to heterogeneous nucleation, where the atoms in the liquid adjacent to a crystalline substrate become layered, exhibiting substantial in-plane atomic ordering within a few atomic layers [38,42]. This prenucleation will lead to the formation of a 2 dimensional (2D) ordered structure at the liquid–substrate interface and have a significant influence on the subsequent heterogeneous nucleation process during solidification [39,40,43]. From molecular dynamics (MD) and density functional theory (DFT) simulations, it has been confirmed that reducing the lattice misfit between the substrate and the solid [38] and the atomic level surface roughness of substrate [45], increasing attractive interaction (negative ΔH_{mix}) between substrate and liquid atoms [49] can significantly enhance the formation of such 2D ordered structure and eventually promote the nucleation potency.

The epitaxial nucleation model [41] represents an atomistic mechanism for heterogeneous nucleation, which proposes that the heterogeneous nucleation proceeds layer-by-layer through structural templating at the liquid–substrate interface. It suggests that nucleation undercooling (ΔT_{n}) is strongly dependent on the lattice misfit (f) between the solid and the substrate. Recently, from MD simulations, it is suggested that heterogeneous nucleation can be best described by a 3-layer nucleation mechanism [39,40,43,44]: the first two layers accommodate misfit, and the third layer creates a crystal plane of the solid (the 2D nucleus) that can template further growth. Meanwhile, the atomistic simulations [43,44] reveal that heterogeneous nucleation undercooling increases linearly with the increase in lattice misfit, which is in good agreement with Fan's epitaxial nucleation theory [41].

2.2. Effect of Solute Segregating at the Liquid/Substrate Interface

In order to minimise the energy of the liquid–substrate interface, solutes may segregate on the surface of the substrate [65–67]. Here, the term "substrate" is defined as any solid particle present in the melt that may act as a potential nucleation site, such as oxides, borides and carbides. Such segregation is most likely a monoatomic layer, only occasionally two or more layers [66,67], and may play a critical role in the heterogeneous nucleation process [55,68], since it may change the atomic arrangement at the liquid–substrate interface (thus misfit) [39,40], surface roughness [45] and chemical potential [49], altering the nucleation potency of the substrate and eventually changing grain size [20].

The recent MD simulations [39,40,43,44], revealing the relationship between heterogeneous nucleation undercooling and lattice misfit, suggest that the nucleation potency of a substrate can be manipulated by the segregation of solute atoms at the liquid–substrate

interface. One of the practical examples is Ti segregation at the liquid–TiB_2 interface. MD simulations [69,70] have suggested that an Al_3Ti-like thin layer could form on the TiB_2 surface due to the segregation of Ti in the melt. Fan et al. [36] experimentally observed the formation of a monoatomic layer of (112) Al_3Ti 2-dimensional compound (2DC) on the (0001) TiB_2 surface. This Al_3Ti 2DC significantly reduces the absolute lattice misfit from −4.22% (between the TiB_2 (0001) terminal surface and the α-Al) to only 0.09% (between the Al_3Ti 2DC and the α-Al), making the TiB_2 with Al_3Ti 2DC extremely potent for nucleating α-Al [36]. It should be noted that not all solute segregations on the substrate surface could reduce the lattice misfit between the substrate and the solid. For example, when Zr is added to Al-alloys inoculated with Al-Ti-B grain refiner, the Al_3Ti 2DC on the TiB_2 becomes thermodynamically unstable and dissolves into the melt [37]. Then, Zr atoms can segregate at the liquid–TiB_2 interface leading to the formation of (0001) Ti_2Zr 2DC on the (0001) TiB_2 surface, changing the absolute lattice misfit back to 4.2% (between Ti_2Zr 2DC and α-Al), which renders TiB_2/Ti_2Zr particles impotent for nucleation of α-Al [37]. Besides the 2DC, segregation of solute at the liquid–substrate interface can also form a 2D solid solution phase (2DS). For example, in Al-5Ti-1B grain refiner inoculated Al-alloys with high contents of Si, the original Al_3Ti 2DC on TiB_2 particle becomes thermodynamically unstable and gradually dissolves into the melt when Si increases to a level of more than 3wt.%; the Al_3Ti 2DC is eventually replaced by Si-rich 2DS, resulting in a reduced nucleation potency [71].

Furthermore, increasing the surface roughness of a crystalline substrate at an atomic level can reduce prenucleation on the substrate [45], which suggests that heterogeneous nucleation can be impeded by roughening the substrate surface at the atomic level. The DFT simulations showed that MgO particle with both {1 1 1} and {0 0 1} terminated faces had an atomically rough surface in liquid Mg [46], as well as α-Al_2O_3{0 0 0 1} and MgO {1 1 1} in liquid Al [47]. This atomically rough terminating layer deteriorates the atomic ordering in the liquid adjacent to the liquid–substrate interface, hence reducing the nucleation potency of the substrates. In addition to lattice misfit and atomic level surface roughness, the chemical interaction between the liquid and the substrate may also affect prenucleation, as Fang et al. [49] found that for a given liquid metal, an attractive chemical interaction (negative heat of mixing) between the liquid and the substrate strengthened atomic ordering in the liquid at the interface, while a repulsive interaction (positive heat of mixing) weakened atomic ordering. Therefore, the segregation of solute at the liquid–substrate interface may change the surface roughness and interaction between substrate and liquid and consequently change the nucleation potency. It should be pointed out that an atomic rough surface of a substrate means higher interfacial energy between the liquid and the substrate, which in turn increases the tendency for segregation of solute elements at such interface due to the increased driving force.

2.3. Effect of Solute on the Formation of New Nucleant Particles

Some solute elements, no matter alloying elements or impurity elements, may change the nucleant particles or lead to the formation of intermetallics prior to α-Al during solidification. Such particles may act as nucleation sites for subsequent solidification of α-Al, and therefore, have a significant influence on the final grain size. For example, 0.7wt.% or more Mg addition in commercial Al (CP-Al) can change the dominant oxide particles from Al_2O_3 in CP-Al to $MgAl_2O_4$ in Al-Mg alloys, which can act as the heterogeneous nucleant particle for α-Al [72]; Ca addition in a twin-roll-cast Mg-3Al-1Zn alloy leads to the formation of Al_2Ca particles during solidification, which was confirmed to nucleate α-Mg and cause grain refinement of AZ31 alloy by Jiang et al. [73]. The formation of primary solid particles is also commonly found in peritectic alloy systems, such as Mg-Zr alloys and Al-Ti alloys, where the particles formed via peritectic reaction in hyper-peritectic alloys may act as heterogeneous nucleation sites, resulting in potential grain refinement. For instance, Wang et al. [74,75] found high-purity commercial Al (HP-Al) was significantly refined by additions of peritectic-forming elements, e.g., Ti, Zr, Nb and V, due to the formation of intermetallics that could act as the nucleation sites for α-Al. The newly formed nucleant

particles due to the addition of solute during the melting or solidification process will introduce the competition for nucleation and grain initiation during solidification [76,77], which strongly affect the final grain size.

2.4. Effect of Solute on Particle Agglomeration

In addition, as the agglomeration of nucleant particles has a strong effect on the final grain size [78], the solute in the melt may affect the grain size by altering the degree of agglomeration of nucleant particles. For example, increasing Mg content in Al-Mg alloy can make the $MgAl_2O_4$ particles self-dispersion throughout the melt [72]. Therefore, this issue is probably a factor affecting final grain size and should be carefully attended to when comparing the solute effect on the grain size.

3. Effect of Solute Growth Restriction on Grain Refinement

3.1. Growth Restriction Parameter β

Although a number of parameters have been proposed to quantify the growth restriction of solutes, such as the constitutional supercooling parameter, P [23], growth restriction factor, Q [14,17], and diffusion coefficient weighted growth restriction factor, U [79], the correlation between these parameters and grain size has been obtained from experiments and modelling [11–13,17,22,24,25]. However, there are still some conflicts not only in the relationships between grain size and these parameters [29,30], but also in the relationships between grain size and Q [19,28]. For example, most of the research shows the grain size is inversely proportional to the growth restriction factor Q, but some other results from both modelling [19] and experiment [28] revealed that the grain size could be simply related to $(1/Q)^{1/3}$. As illustrated in Figure 1 and described by Equations (1) and (2), the P and Q are more likely thermodynamic parameters, which are ineffective to describe the growth restriction of solute at different solidification processes, i.e., different cooling rates:

$$P = \frac{mC_0(k-1)}{k} \tag{1}$$

$$Q = mC_0(k-1) \tag{2}$$

where m is the slope of liquidus, C_0 is the solute concentration and k is the partition coefficient. Based on an analytical model, we [80] proposed a growth restriction parameter, β, to quantify the growth restriction of solute:

$$\beta = \frac{mC_0(k-1)}{\Delta T} - k \tag{3}$$

which contains not only the thermodynamic part, $mC_0(k-1)$, but also the kinetic part, ΔT.

For diffusion-controlled spherical growth, the growth velocity V of a grain of radius r is given by the following equation [81,82]:

$$V = \frac{\lambda^2 D}{2r} \tag{4}$$

where D is the diffusion coefficient of solute and λ is a parameter related to the instantaneous undercooling. If $\lambda^2/2$ is taken as the growth coefficient, its inverse, $2/\lambda^2$, can be considered as the growth restriction coefficient. As shown in Figure 2 [80], $2/\lambda^2$ is a monotonical function of β and independent of the nature of solutes. In addition, the β also can be expressed as the following equation:

$$\beta = \frac{f_L}{f_S} \tag{5}$$

where f_L and f_S are the phase fractions of the liquid and the solid, respectively. Equation (5) indicates the physical meaning of β is the ratio of the liquid phase fraction, f_L, to the

solid phase fraction, f_S. Furthermore, Equation (5) provides an approach to calculating the true β values of multicomponent systems using CALPHAD software and associated thermodynamic databases.

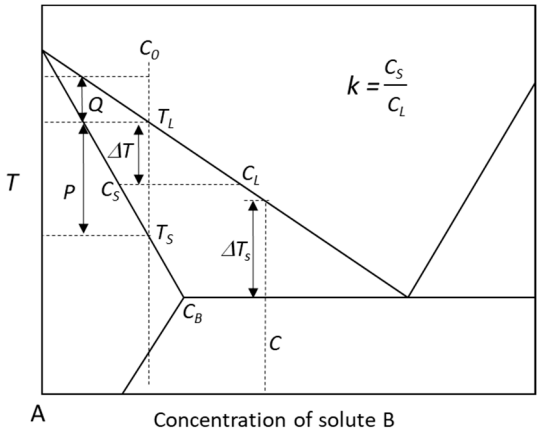

Figure 1. Schematic phase diagram of a binary A-B system showing the definitions of the relevant parameters related to growth restriction, such as P, Q and ΔT_s. When $C_0 \leq C_B$, $P = \Delta T_s$; when $C_0 > C_B$, $P > \Delta T_s$, e.g., C_0 = C.

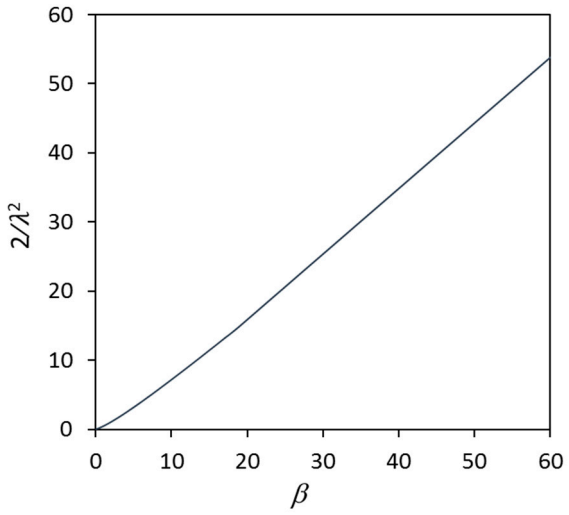

Figure 2. Growth restriction coefficient ($2/\lambda^2$) for spherical growth during solidification of binary alloys as a function of the growth restriction parameter, β, showing that the growth restriction coefficient is a unique function of β, regardless of the nature of solutes, solute concentrations and solidification conditions. Reprinted with permission from Ref. [80]. Copyright 2022 Elsevier.

However, it should be noted that there is a critical undercooling (ΔT in Equation (3)) below which the solidification becomes non-diffusion controlled. This means that there is a critical concentration (C^*) for a given alloy, beyond which the solidification will be diffusion-controlled, and the solute will partition between the solid and liquid phases during the growth of the solid phase [80]; otherwise, solidification will no longer be diffusion-controlled, and there is no partitioning of solute during the growth of solid phase, meaning there is no growth restriction of solute. Taking a binary alloy solidifying under a given undercooling (ΔT), for example, one obtains C^* from Equation (3):

$$C^* = \frac{k\Delta T}{m(k-1)}. \quad (6)$$

Equation (6) suggests that C^* increases with increasing ΔT for a given binary alloy. Clearly, C^* marks the solute concentration at which the solidification undercooling equals

the freezing range of the alloy no matter the eutectic and peritectic systems. For a given undercooling ΔT, when $C_0 < C^*$, solidification becomes partitionless (non-equilibrium solidification), and therefore there is no growth restriction ($\beta = 0$); whereas when $C_0 > C^*$, growth restriction increases with increasing C_0, as described by Equation (3). It is very likely that partitionless solidification occurs in the systems, such as Al-Zr and Mg-Mn alloys, where the maximum freezing ranges of these alloys ($C_0 < C_m$) are very small, being about 0.2 K for Al-Zr alloys and 0.1 K for Mg-Mn alloys (calculated from the Pandat software with PanAl database and PanMg database [83]), which are in the range of undercooling of the standard TP-1 test (about 0.5 K) [84]. Therefore, the growth restriction of solute is only applicable in the condition that the growth undercooling is smaller than the freezing range of the alloy.

3.2. Effect of Growth Restriction on Columnar to Equiaxed Transition (CET)

Grain refinement aims to suspend columnar grain growth and form a fine equiaxed grain structure throughout the ingots or castings [3]. The first target of grain refinement is to achieve columnar to equiaxed transition (CET) [3]. CET requires the equiaxed grains formed at the solidification front can effectively block the growth of columnar dendrites, which is referred to as the front blocking mechanism proposed by Hunt [85]. As illustrated in the schematical CET map (Figure 3), there are three types of as-cast microstructures, columnar, equiaxed and mixed grain structure, depending on temperature gradient (G) and growth velocity (V). Figure 3 suggests that equiaxed grain structures are favoured by high growth velocity, high solute concentration and low temperature gradient. Under a quasi-isothermal (G is very small) condition, such as the standard TP-1 test, the as-cast structure is more likely to be either equiaxed or columnar, as the mixed zone becomes very limited under this condition, as shown in the dashed box in Figure 3. For example, the TP-1 samples of Al binary alloys with sufficient grain refiner showed either columnar structure or equiaxed structure [86,87].

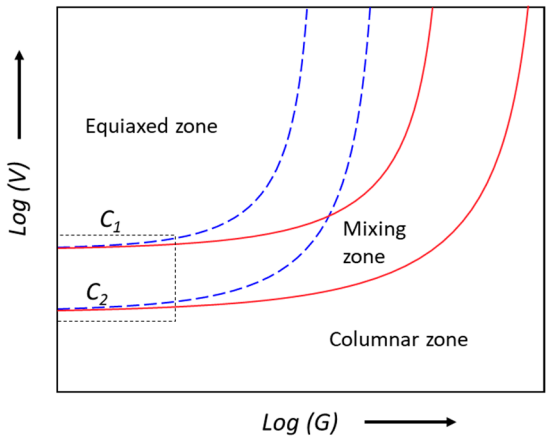

Figure 3. Schematic diagram illustrating the Hunt CET map for two alloys with compositions of C_1 and C_2 ($C_1 < C_2$), showing three zones: columnar zone, equiaxed zone and mixing zone (between the blue and red lines). The dashed box shows the area with very low temperature gradient (G).

Based on the front blocking mechanism of CET, we proposed a criterion for CET under a quasi-isothermal solidification [9]:

$$\beta = 1.14. \ (G \rightarrow 0) \tag{7}$$

when $\beta = 1.14$ the CET will occur during solidification; $\beta > 1.14$, the as-cast alloy will be a fully equiaxed grain structure; $\beta < 1.14$, the as-cast alloy will be a fully columnar grain structure. This criterion was validated using the standard TP-1 test not only in binary Al alloys but also in some ternary systems, e.g., Al-Fe-Si and Al-Fe-Cu systems, as shown

in Figure 4 [9,87], where the concentrations for CET predicted by β = 1.14 are in good agreement with that obtained by experiments. However, it should be noted that β = 1.14 as a criterion for CET is only applicable to solidification conditions where the temperature gradient is very small, i.e., $G \rightarrow 0$ [9].

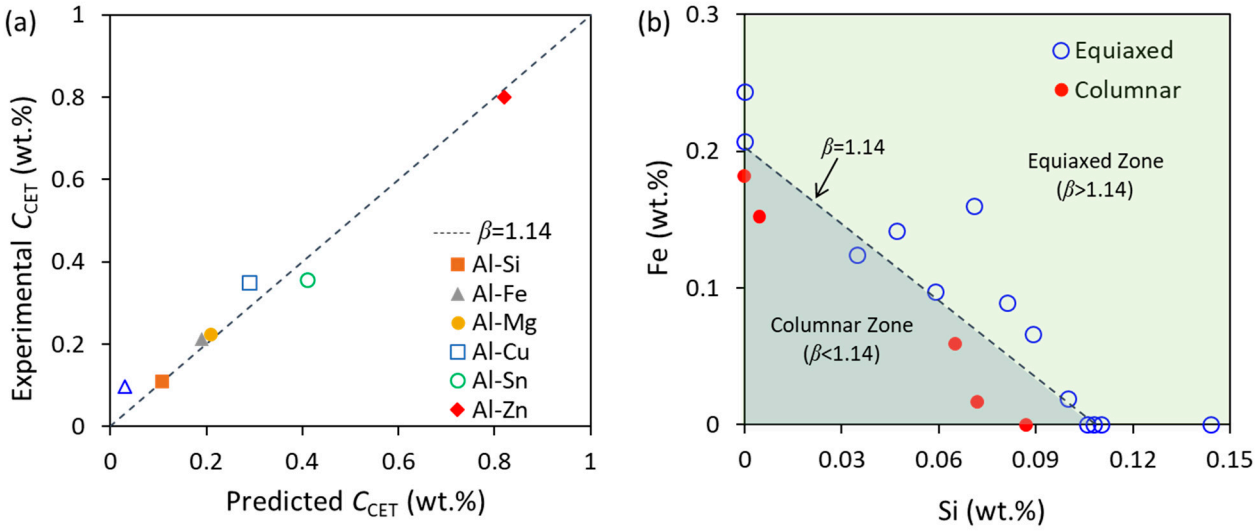

Figure 4. Comparison between the predicted composition for CET by β = 1.14 and the experimental results from the standard TP-1 test [9,87]. (**a**) Binary Al alloys and (**b**) Al-Fe-Si ternary alloys. Reprinted with permission from Ref. [9]. Copyright 2022 Elsevier.

3.3. Effect of Growth Restriction on Grain Size

Grain refinement is a complex phenomenon involving many factors that are operational simultaneously, such as alloy compositions and the chemical and physical nature of nucleant particles, which may include crystal structure, morphology, surface termination, size distribution and number density. In order to correctly evaluate the growth restriction of solute on grain size, other conditions should be kept constant. We have carried out a series of rigorous experiments to assess the growth restriction effect of solute on grain size in Al and Mg binary alloys [9,87]. Some key information for the experiment is shown as follows:

(1) *Using an excess-Ti-free grain refiner for Al alloys*: To eliminate the influence of excess Ti (introduced from Al-5Ti-1B grain refiner), a new grain refiner alloy, Al-1.54TiB_2 [87], was produced by repeated dilution–filter–dilution of the commercial Al-5Ti-1B grain refiner using HP-Al. The resultant Al-1.54TiB_2 master alloy contains only Al_3Ti 2DC sheathed TiB_2 particles with other impurities being reduced to a few ppm. In each Al binary alloy, the same amount of potent TiB_2 particles was added, approximately 10^{13} m^{-3}.

(2) *Applying intensive melt shearing for Mg alloys*: An intensive melt shearing technique [88–91] was adopted in Mg binary alloys, which can effectively disperse MgO particles to ensure a nearly consistent total number density throughout the melt prior to solidification processing. The particle number density in the fully sheared melt is estimated to be 10^{17} m^{-3}, compared with 10^{14} m^{-3} in the non-sheared melts [92].

(3) *Using standard TP-1 test to standardise solidification condition*: The standard Alcan TP-1 test [84] provides a quasi-isothermal solidification with a constant cooling rate (3.5 K/s) at the centre of the sample for Al and Mg alloys.

(4) *Checking microstructure in both vertical and cross sections*: The grain size is only meaningful for equiaxed grain structures. To ensure grain size is measured only for equiaxed grain structures, both vertical and cross sections of TP-1 samples were checked, as some samples that show an equiaxed structure in cross section may be columnar

when the vertical section is checked. This will avoid the inaccuracy introduced by the "grain size" data measured from the columnar structures.

From the experimental results by Spittle and Sadli [24], the grain size of Al alloys decreased dramatically from about 1200 μm for HP-Al to about 110 μm with increasing solute content. However, the alloys with large grain sizes (larger than 400 μm) are mainly located in the region of $\beta < 1.14$ (Figure 5a [9]). From the CET criterion, the alloys within the region of $\beta < 1.14$ have a columnar structure, which was confirmed by the repeated experiment [9]. Therefore, these samples that show columnar structures should be eliminated for assessing the growth restriction effect on grain size.

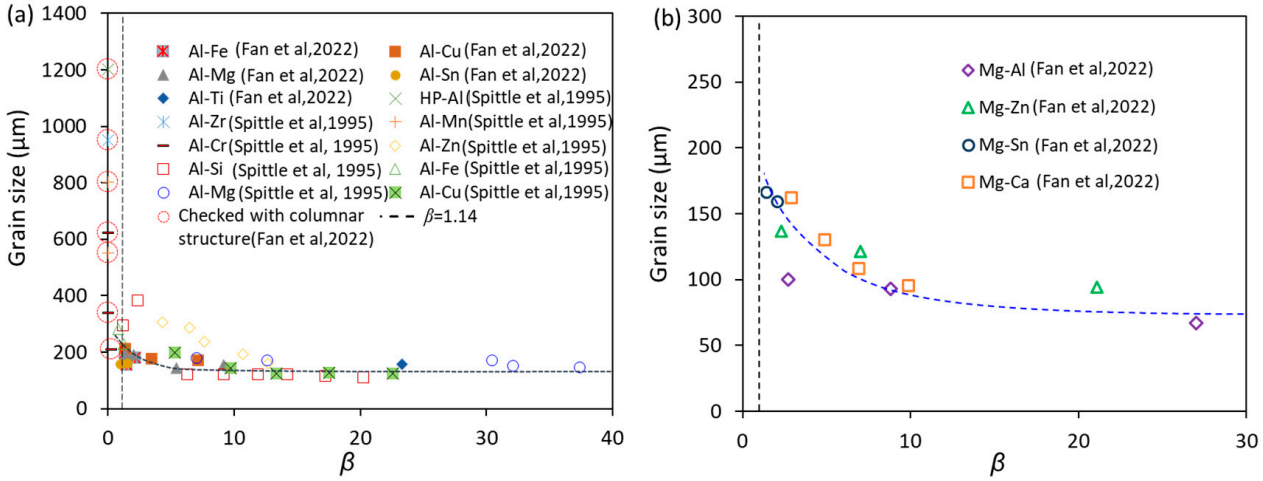

Figure 5. Experimentally measured grain size as a function of growth restriction parameter, β, in (**a**) Al alloys and (**b**) Mg alloys [9]. The grain size was measured from TP-1 test samples of Al alloys inoculated with the potent TiB_2 particles (number density of 10^{13} m^{-3}) and Mg alloys with intensive melt shearing (MgO number density is 10^{17} m^{-3}). Experimental data are from Refs. [9,24].

The microstructure changes abruptly from columnar to equiaxed around $\beta = 1.14$ (Figure 5) [9], which means necessary growth restriction is needed for achieving grain refinement, allowing the occurrence of CET. After CET, growth restriction has a moderate effect on the reduction of grain size, as shown in the range of $1.14 < \beta < 15$ in Figure 5, which shows the experimental data in Al (Figure 5a) and Mg alloys (Figure 5b) assessed by the TP-1 tests; further increase in growth restriction when $\beta > 15$ will have almost no effect on the grain size. The exaggerated conclusion in the literature that solute has a significant effect on grain size is most likely caused by the inclusion of erroneous grain size data of dilute alloys that have a columnar grain structure. The numerical calculations showing the growth restriction effect on grain size in Al-Cu, Al-Fe and Al-Si alloys inoculated with Al-1.54TiB_2 grain refiner solidified under the same solidification conditions also confirm that grain size decreases with increasing β when $\beta < 20$, and levels off when $\beta > 20$ (Figure 6 [9]).

To further analyse the mechanism of growth restriction on grain refinement, the solidification behaviours of Al-Cu alloys that contain the same nucleant particles (constant number density and size distribution) were investigated (Figure 7 [9]). Increasing the growth restriction of solute in the melt, the growth velocity of the solid phase will decrease, resulting in a delay of recalescence (Figure 7a). As a result, the maximum undercooling obtained at recalescence, ΔT_{max}, increases (Figure 7b), which leads to an increase in grain initiation events (N_{gi}) (Figure 7c), and hence a reduction of grain size ($\bar{d}$) (Figure 7d). The number of grain initiation events increases, and the grain size decreases with increasing solute contents at low Cu concentrations, while the change of grain size levels off at high Cu concentrations since grain size ($\bar{d}$) is related to N_{gi} through the following equation [17]:

$$\bar{d} = \frac{0.5}{(N_{gi})^{1/3}} \quad (8)$$

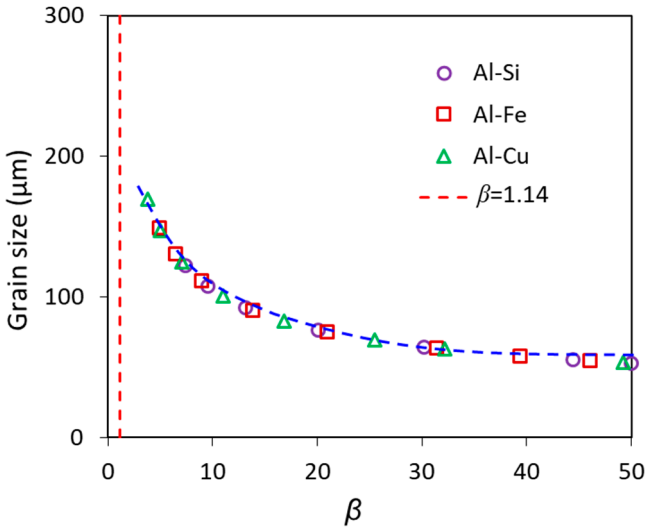

Figure 6. Calculated grain size as a function of growth restriction parameter, β, for Al alloys inoculated by potent TiB_2 particles ($N_0 = 1 \times 10^{13}$ m^{-3}) with a log-normal size distribution ($d_0 = 0.67$ μm and $\sigma = 0.876$) at $\dot{T} = 3.5$ K/s [9]. Reprinted with permission from Ref. [9]. Copyright 2022 Elsevier.

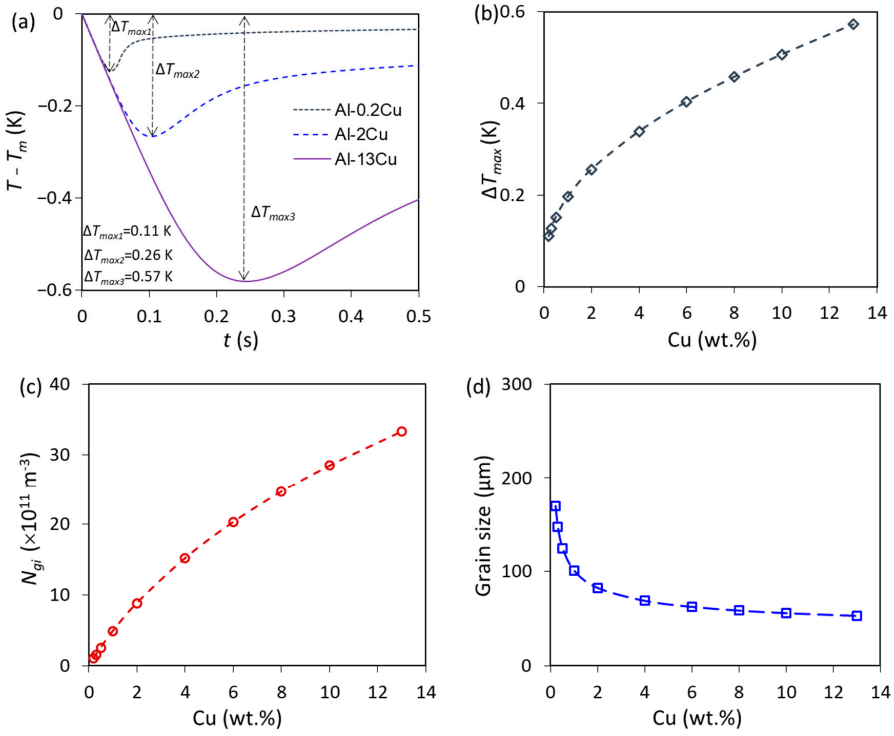

Figure 7. The calculations of Al-Cu alloys inoculated by potent TiB_2 particles ($N_0 = 1 \times 10^{13}$ m^{-3}) with a log-normal size distribution ($d_0 = 0.67$ μm and $\sigma = 0.876$) at $\dot{T} = 3.5$ K/s [9]. (**a**) The calculated cooling curves of Al-0.2Cu, Al-2Cu and Al-13Cu alloys, showing that recalescence is delayed to a lower temperature by increasing the solute contents; (**b**) the calculated ΔT_{max}, (**c**) the total number density of initiated grains (N_{gi}); and (**d**) the predicted grain size. Reprinted with permission from Ref. [9]. Copyright 2022 Elsevier.

In brief summary, the mechanism of growth restriction effect on grain size is that, when all other parameters are kept constant, an increase in solute concentration slows down crystal growth due to solute growth restriction, which in turn increases the max undercooling achievable at recalescence and allows more nucleant particles to participate

in grain initiation, consequently resulting in an increased total number of grain initiation events and thus reduced grain size.

3.4. Growth Restriction in the Case of Explosive Grain Initiation (EGI)

As demonstrated in Ref. [35], the grain initiation mode of the Al alloys inoculated by potent TiB_2 particles in the TP-1 test is a typical PGI. However, the growth restriction effect on grain size for EGI is different from that for PGI. The grain refinement map of the ΔT_n-C_0 (nucleation undercooling-composition) plot (Figure 8a) [20] shows the growth restriction effect on grain size in PGI-dominant and EGI-dominant zones, which are delineated by a line that represents the solidification conditions where the number of EGI and PGI events are equal. In the PGI-dominant zone (light shadow in Figure 8a), grain size decreases with increasing solute contents, while in the EGI-dominant zone (dark shadow in Figure 8a) grain size is almost independent of solute contents as suggested by the vertical iso-grain-size lines, which is more clearly shown in Figure 8b. This indicates the growth restriction effect of solute on grain size becomes weaker with increasing the EGI event during solidification.

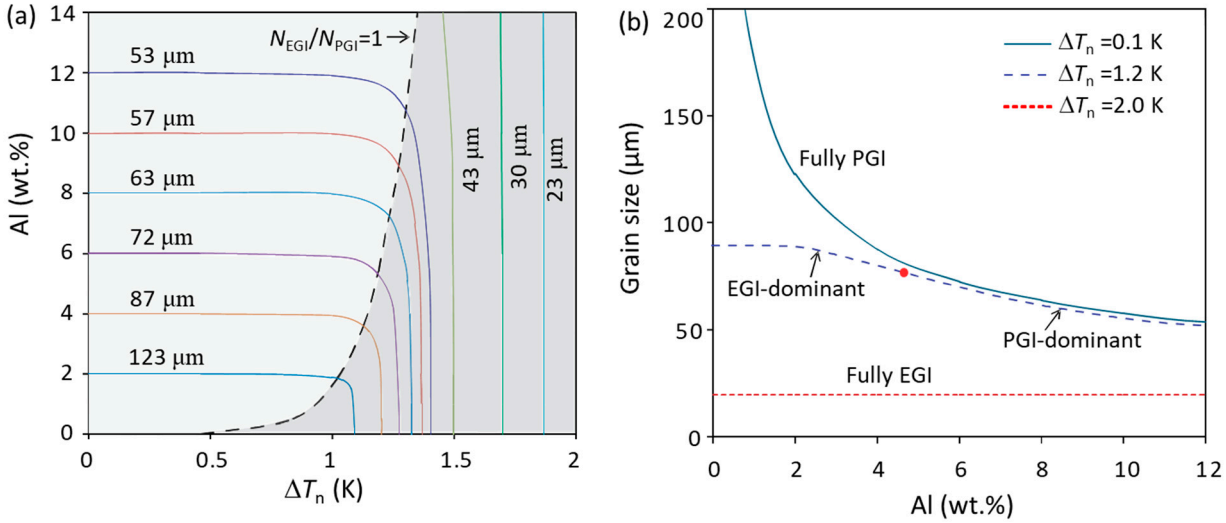

Figure 8. (**a**) Grain refinement map of the ΔT_n-C_0 (nucleation undercooling-composition) plot and (**b**) solute effect on grain size for Mg-Al alloys with particle number density 10^{17} m^{-3} and a log-normal size distribution (d_0 = 0.67 μm and σ = 0.876) at $\dot{T}$ = 3.5 K/s [20].

4. Discussion

4.1. Atomistic Mechanism of Growth Restriction

Because of the partitioning of solute elements between the solid and liquid phases during solidification and the difference in diffusivity of solute in the melt, solute elements will redistribute at the solid–liquid interface and then result in the enrichment/depletion of solute at the solid–liquid interface, which leads to the decrease in velocity of the solid–liquid interface, showing the growth restriction effect of solute. However, the physical mechanism at the atomic level is worthy of further consideration. The growth velocity of the solid phase is determined by the competition between the atomic attachment and detachment, which is related to the driving force of the phase transformation from liquid to solid, and the rate of supply of such atoms to the solid–liquid interface from the bulk liquid. Kinetically, as the atomic attachment and detachment at the interface are easy under relatively small undercooling within a very small time scale, the controlling factor for growth is the rate of atomic supply from the bulk liquid to the solid–liquid interface. For the alloys containing eutectic-forming elements (k < 1), the controlling factor for solid growth is the supply of the solvent atoms to the interface during solidification. The solute atoms will enrich at the solid–liquid interface due to the rejection of solute atoms from the solid phase, which will block the supply of solvent atoms and consequently lead to a decreased growth velocity. On the contrary, for the alloys containing peritectic-forming

elements ($k > 1$), the growth of the solid phase needs more solute atoms causing a depletion of solute (equivalent to the enrichment of solvent) at the solid–liquid interface. Then, the supply of solute atoms becomes the controlling factor for solid growth. In this case, the solvent atoms enriched at the solid–liquid interface will block the supply of solute atoms, leading to a decreased growth velocity of the solid. Therefore, the physical origin of growth restriction is the blockage of the supply of the critical elements for solid growth, i.e., solvent atoms in the case of eutectic-forming elements and solute atoms in the case of peritectic-forming elements.

4.2. Enhancing Grain Refinement

From Section 3, it is clear that the growth restriction of solute is required for grain refinement, as it can induce the CET during solidification to achieve an equiaxed structure. After CET, the grain size is only moderately reduced with initially increasing growth restriction of solute, and the reduction becomes very limited when the growth restriction reaches a certain level, such as $\beta > 15$ in Figure 5. Therefore, the approach to achieve significant grain refinement via increasing growth restriction of the alloys is not so effective in the practical solidification conditions, especially when the alloys already have sufficient growth restriction.

When the alloys are inoculated by a grain refiner with potent nucleant particles, the grain initiation is treated as PGI. For example, in the solidification process of Al-Cu alloys inoculated with 1 ppt (0.1 wt%) Al-5Ti-1B grain refiner [35], the TiB_2 particles with Al_3Ti 2DC on the surface show an extremely high nucleation potency with nucleation undercooling (ΔT_n) around 0.01 K [17]. The approach that promotes PGI to achieve grain refinement has reached its limit leaving little space for further improvement [18,20,35]. On the other hand, the concept of EGI provides a new approach that has the potential to push grain refinement to a level unachievable by PGI [20,34,35]. It has been demonstrated by a numerical modelling that impeding heterogeneous nucleation (increasing ΔT_n), promoting EGI, can significantly reduce the grain size when other conditions are fixed constantly [20,34,35]. As mentioned in Section 2, the solute segregated on the surface of the nucleant particle may change the nucleation potency due to the variation in lattice misfit, surface roughness and chemical potential, which provide an approach to achieving significant grain refinement by manipulating the nucleation potency of particles. For example, the Mg alloys provide us with a potential alloy system to apply this new approach.

The native MgO particles are the only dominant inclusions in the Mg melt [88,93], which can be effectively dispersed throughout the melt using intensive melt shearing, and the number density can be as high as 10^{17} m^{-3} level [92]. The MgO has a large lattice misfit with α-Mg (7.9%) [93], indicating the nucleation undercooling of MgO for α-Mg is relatively large compared to potent TiB_2 particle for α-Al and Zr particle for α-Mg. This makes MgO particularly effective for grain refinement of Mg alloys through the promotion of EGI. In addition, the first principal calculations show that the elements, e.g., Ca, Be, Sr and Ba, are readily adsorbed on the surface of MgO [94]. Wang et al. [95,96] experimentally observed an adsorption layer at the Mg/MgO interface when Ca and Sn were added to the Mg melt, which may lead to atomic surface roughness and then change the nucleation potency of MgO particle. Therefore, to achieve significant grain refinement by "poisoning" the native oxides with the addition of minor solute to induce the chemical segregation at the liquid–oxide interface is of importance for both the development of grain refinement and the closed-loop recycling of metallic materials, as it not only makes native inclusions useful and effective for grain refinement, but also significantly reduces the probability for the existence of large inclusions, having a positive effect on final mechanical performance, especially for secondary alloys.

5. Summary

Although extensive research has been carried out on the solute effect on grain refinement and significant progress has been made over the past decades, there are still some

key questions that remain open. Heterogeneous nucleation and grain initiation are two important processes at the early stage of solidification related to the final grain size. In this paper, we have briefly reviewed the solute effect on heterogeneous nucleation via segregation on the surface of the substrate or the formation of nucleant particles. Then, we present an overview of the growth restriction effect of solute on grain refinement, and the key points are shown as follows:

(1) The growth restriction parameter, β, is a function of C_0, m, k and ΔT, incorporating holistically the nature of solute, solute concentration and solidification condition. The physical meaning of β is the ratio of the liquid phase fraction, f_L, to the solid phase fraction, f_S.

(2) Theoretically, for a given alloy system solidifying under a given undercooling, there is a critical solute concentration (C^*), below which solidification becomes partitionless (non-equilibrium solidification), and therefore there is no growth restriction ($\beta = 0$) during solidification.

(3) The key role of growth restriction on grain refinement is to achieve the equiaxed structure of as-cast alloys. Under quasi-isothermal solidification condition, a CET criterion is developed: $\beta = 1.14$. When $\beta < 1.14$, the as-cast microstructure is most likely columnar; and when $\beta > 1.14$, the as-cast microstructure will be equiaxed.

(4) For progressive grain initiation, the grain size is moderately reduced with an increase in growth restriction just after CET, and levels off with further increase in growth restriction. For explosive grain initiation, the growth restriction has no effect on the grain size.

(5) The traditional approach that promotes PGI by the addition of grain refiner with potent nucleant particles to achieve grain refinement has reached its limit leaving little space for further improvement. However, impeding heterogeneous nucleation (increasing ΔT_n), promoting EGI, may achieve significant grain refinement.

Author Contributions: Conceptualization, Z.F. and F.G.; methodology, F.G.; formal analysis, F.G.; investigation, F.G.; resources, F.G.; data curation, F.G.; writing—original draft preparation, F.G.; writing—review and editing, Z.F.; visualization, F.G.; supervision, Z.F.; project administration, Z.F.; funding acquisition, Z.F. All authors have read and agreed to the published version of the manuscript.

Funding: This work was financially supported by the EPSRC (UK) under grant number EP/N007638/1.

Data Availability Statement: Not applicable.

Conflicts of Interest: The authors declare no conflict of interest.

References

1. Polmear, I.; StJohn, D.; Nie, J.F.; Qian, M. (Eds.) *Light Alloys: Metallurgy of the Light Metals*; Butterworth-Heinemann: Oxford, UK, 2017.
2. Dobrzański, L.A.; Totten, G.E.; Bamberger, M. (Eds.) *Magnesium and Its Alloys: Technology and Applications*; CRC Press: Boca Raton, FL, USA, 2020.
3. McCartney, D.G. Grain refining of Al and its alloys using inoculants. *Int. Mater. Rev.* **1989**, *34*, 247–260. [CrossRef]
4. Cantor, B.; O'Reilly, K. (Eds.) *Solidification and Casting*; The Institute of Physics: London, UK, 2003.
5. Cibula, A. The mechanism of grain refinement of sand castings in Al alloys. *J. Inst. Met.* **1949**, *76*, 321–360.
6. Easton, M.; Stjohn, D. Grain refinement of aluminum alloys: Part I. the nucleant and solute paradigms-a review of the literature. *Metall. Mater. Trans. A* **1999**, *30*, 1613–1623. [CrossRef]
7. Lee, Y.C.; Dahle, A.K.; StJohn, D.H. The role of solute in grain refinement of magnesium. *Metall. Mater. Trans. A* **2000**, *31*, 2895–2906. [CrossRef]
8. StJohn, D.H.; Qian, M.A.; Easton, M.A.; Cao, P.; Hildebrand, Z. Grain refinement of magnesium alloys. *Metall. Mater. Trans. A* **2005**, *36*, 1669–1679. [CrossRef]
9. Fan, Z.; Gao, F.; Wang, Y.; Men, H.; Zhou, L. Effect of solutes on grain refinement. *Prog. Mater. Sci.* **2022**, *123*, 100809. [CrossRef]
10. Murty, B.S.; Kori, S.A.; Chakraborty, M. Grain refinement of aluminium and its alloys by heterogeneous nucleation and alloying. *Int. Mater. Rev.* **2002**, *47*, 3–29. [CrossRef]
11. Greer, A.L. Overview: Application of heterogeneous nucleation in grain-refining of metals. *J. Chem. Phys.* **2016**, *145*, 211704. [CrossRef]
12. Easton, M.A.; Qian, M.; Prasad, A.; StJohn, D.H. Recent advances in grain refinement of light metals and alloys. *Curr. Opin. Solid State Mater. Sci.* **2016**, *20*, 13–24. [CrossRef]

13. Liu, Z. Review of grain refinement of cast metals through inoculation: Theories and developments. *Metall. Mater. Trans. A* **2017**, *48*, 4755–4776. [CrossRef]
14. Maxwell, I.; Hellawell, A. A simple model for grain refinement during solidification. *Acta Metall.* **1975**, *23*, 229–237. [CrossRef]
15. Rutter, J.W.; Chalmers, B. A prismatic substructure formed during solidification of metals. *Can. J. Phys.* **1953**, *31*, 15–39. [CrossRef]
16. Tiller, W.A.; Jackson, K.A.; Rutter, J.W.; Chalmers, B. The redistribution of solute atoms during the solidification of metals. *Acta Metall.* **1953**, *1*, 428–437. [CrossRef]
17. Greer, A.L.; Bunn, A.M.; Tronche, A.; Evans, P.V.; Bristow, D.J. Modelling of inoculation of metallic melts: Application to grain refinement of Al by Al-Ti-B. *Acta Mater.* **2000**, *48*, 2823–2835. [CrossRef]
18. Quested, T.E.; Greer, A.L. Effect of the size distribution of inoculant particles on as-cast grain size in Al alloys. *Acta Mater.* **2004**, *52*, 3859–3868. [CrossRef]
19. Men, H.; Fan, Z. Effects of solute content on grain refinement in an isothermal melt. *Acta Mater.* **2011**, *59*, 2704–2712. [CrossRef]
20. Fan, Z.; Gao, F.; Jiang, B.; Que, Z.P. Impeding nucleation for more significant grain refinement. *Sci. Rep.* **2020**, *10*, 9448. [CrossRef]
21. Qian, M.; Cao, P.; Easton, M.A.; McDonald, S.D.; StJohn, D.H. An analytical model for constitutional supercooling-driven grain formation and grain size prediction. *Acta Mater.* **2010**, *58*, 3262–3270. [CrossRef]
22. StJohn, D.H.; Qian, M.; Easton, M.A.; Cao, P. The interdependence theory: The relationship between grain formation and nucleant selection. *Acta Mater.* **2011**, *59*, 4907–4921. [CrossRef]
23. Tarshis, L.A.; Walker, J.L.; Rutter, J.W. Experiments on the solidification structure of alloy castings. *Metall. Trans.* **1971**, *2*, 2589–2597. [CrossRef]
24. Spittle, J.A.; Sadli, S.B. Effect of alloy variables on grain refinement of binary Al alloys with Al-Ti-B. *Mater. Sci. Technol.* **1995**, *11*, 533–537. [CrossRef]
25. Spittle, J.A.; Brown, S.G.R. Computer simulation of effects of alloy variables on the grain structures of castings. *Acta Metall.* **1989**, *37*, 1803–1810. [CrossRef]
26. Easton, M.A.; StJohn, D.H. An analysis of the relationship between grain size, solute content, and the potency and number density of nucleant particles. *Metall. Mater. Trans. A* **2005**, *36*, 1911–1920. [CrossRef]
27. Easton, M.A.; StJohn, D.H. Improved prediction of grain size of Al alloys that includes effect of cooling rate. *Mater. Sci. Eng. A* **2008**, *486*, 8–13. [CrossRef]
28. Becerra, A.; Pekguleryuz, M. Effects of zinc, lithium, and indium on grain size of magnesium. *J. Mater. Res.* **2009**, *24*, 1722–1729. [CrossRef]
29. Xu, H.; Xu, L.D.; Zhang, S.J.; Han, Q. Effect of the alloy composition on the grain refinement of Al alloys. *Scr. Mater.* **2006**, *54*, 2191–2196. [CrossRef]
30. Liu, Z.; Wang, F.; Qiu, D.; Taylor, J.A.; Zhang, M.X. Effect of solute elements on the grain refinement of cast Zn. *Metall. Mater. Trans. A* **2013**, *44*, 4025–4030. [CrossRef]
31. Shu, D.; Sun, B.; Mi, J.; Grant, P.S. A quantitative study of solute diffusion field effects on heterogeneous nucleation and grain size of alloys. *Acta Mater.* **2011**, *59*, 2135–2144. [CrossRef]
32. Du, Q.; Li, Y. An extension of the Kampmann-Wagner numerical model towards as-cast grain size prediction of multicomponent Al alloys. *Acta Mater.* **2014**, *71*, 380–389. [CrossRef]
33. Wagner, R.; Kampmann, R. Homogeneous second phase precipitation. In *Materials Science and Technology: A Comprehensive Treatment*; Cahn, R.W., Ed.; John Wiley & Sons, Inc.: Weinheim, Germany, 1991.
34. Fan, Z. Heterogeneous nucleation, grain initiation and grain refinement of Mg-alloys. In *Proceedings of the 11th International Conference on Magnesium Alloys and Their Applications*; Beaumont Estate: Old Windsor, UK, 2018; pp. 7–17.
35. Fan, Z.; Gao, F. Grain initiation and grain refinement: An overview. *Metals* 2022, *in progress*.
36. Fan, Z.; Wang, Y.; Zhang, Y.; Qin, T.; Zhou, X.R.; Thompson, G.E.; Pennycook, T.; Hashimotob, T. Grain refining mechanism in the Al/Al-Ti-B system. *Acta Mater.* **2015**, *84*, 292–304. [CrossRef]
37. Wang, Y.; Fang, C.M.; Zhou, L.; Hashimoto, T.; Zhou, X.; Ramasse, Q.M.; Fan, Z. Mechanism for Zr poisoning of Al-Ti-B based grain refiners. *Acta Mater.* **2019**, *164*, 428–439. [CrossRef]
38. Men, H.; Fan, Z. Prenucleation induced by crystalline substrates. *Metall. Mater. Trans. A* **2018**, *49*, 2766–2777. [CrossRef]
39. Fan, Z.; Men, H. A molecular dynamics study of heterogeneous nucleation in generic liquid/substrate systems with positive lattice misfit. *Mater. Res. Express* **2020**, *7*, 126501. [CrossRef]
40. Fan, Z.; Men, H.; Wang, Y.; Que, Z.P. A new atomistic mechanism for heterogeneous nucleation in the systems with negative lattice misfit: Creating a 2D template for crystal growth. *Metals* **2021**, *11*, 478. [CrossRef]
41. Fan, Z. An epitaxial model for heterogeneous nucleation on potent substrates. *Metall. Mater. Trans. A* **2013**, *44*, 1409–1418. [CrossRef]
42. Men, H.; Fang, C.M.; Fan, Z. Prenucleation at the liquid/substrate interface: An overview. *Metals* 2022, *in progress*.
43. Fan, Z.; Men, H. An overview on atomistic mechanisms of heterogeneous nucleation. *Metals* 2022, *in progress*.
44. Fan, Z.; Men, H. Heterogeneous nucleation and grain initiation on a single substrate. *Metals* **2022**, *12*, 1454. [CrossRef]
45. Jiang, B.; Men, H.; Fan, Z. Atomic ordering in the liquid adjacent to an atomically rough solid surface. *Comp. Mater. Sci.* **2018**, *153*, 73–81. [CrossRef]
46. Fang, C.M.; Fan, Z. Prenucleation at the interface between MgO and liquid magnesium: An ab initio molecular dynamics study. *Metall. Mater. Trans. A* **2020**, *51*, 788–797. [CrossRef]

47. Fang, C.M.; Fan, Z. Prenucleation at the liquid-Al/α-Al_2O_3 and the liquid-Al/MgO interfaces. *Comp. Mater. Sci.* **2020**, *171*, 109258. [CrossRef]
48. Fang, C.; Yasmin, S.; Fan, Z. Interfacial interaction and prenucleation at liquid-Al/γ-Al_2O_3 {1 1 1} interfaces. *J. Phys. Comm.* **2021**, *5*, 15007. [CrossRef]
49. Fang, C.M.; Men, H.; Fan, Z. Effect of substrate chemistry on prenucleation. *Metall. Mater. Trans. A* **2018**, *49*, 6231–6242. [CrossRef]
50. Kelton, K.F.; Greer, A.L. (Eds.) *Nucleation in Condensed Matter: Applications in Materials and Biology*; Pergamon: Oxford, UK, 2010.
51. Gibbs, J.W. On the equilibrium of heterogeneous substances. *Am. J. Sci.* **1879**, *16*, 441–458. [CrossRef]
52. Volmer, M.; Weber, A.Z. Nucleus formation in supersaturated systems. *Z. Phys. Chem.* **1926**, *119*, 277–301. [CrossRef]
53. Becker, R.; Döring, W. Kinetic treatment of nucleation in supersaturated vapors. *Ann. Phys.* **1935**, *24*, 719–752. [CrossRef]
54. Zeldovich, J.B. On the theory of new phase formation: Cavitation. *Acta Physicochim.* **1943**, *18*, 1.
55. Cantor, B. Heterogeneous nucleation and adsorption. *Phil. Trans. R. Soc. Lond. A* **2003**, *361*, 409–417. [CrossRef]
56. Gebauer, D.; Völkel, A.; Cölfen, H. Stable prenucleation calcium carbonate clusters. *Science* **2008**, *322*, 1819–1822. [CrossRef]
57. Vekilov, P.G. The two-step mechanism of nucleation of crystals in solution. *Nanoscale* **2010**, *2*, 2346–2357. [CrossRef]
58. Chen, J.; Zhu, E.; Liu, J.; Zhang, S.; Lin, Z.; Duan, X.; Heinz, H.; Huang, Y.; De Yoreo, J.J. Building two-dimensional materials one row at a time: Avoiding the nucleation barrier. *Science* **2018**, *362*, 1135–1139. [CrossRef]
59. Zhou, J.; Yang, Y.; Yang, Y.; Kim, D.S.; Yuan, A.; Tian, X.; Ophus, C.; Sun, F.; Schmid, A.K.; Nathanson, M.; et al. Observing crystal nucleation in four dimensions using atomic electron tomography. *Nature* **2019**, *570*, 500–503. [CrossRef]
60. Oh, S.H.; Kauffmann, Y.; Scheu, C.; Kaplan, W.D.; Ruhle, M. Ordered liquid aluminum at the interface with sapphire. *Science* **2005**, *310*, 661–663. [CrossRef]
61. Kauffmann, Y.; Oh, S.H.; Koch, C.T.; Hashibon, A.; Scheu, C.; Ruhe, M.; Kaplan, W.D. Quantitative analysis of layering and in-plane structural ordering at an alumina-aluminum solid-liquid interface. *Acta Mater.* **2011**, *59*, 4378–4386. [CrossRef]
62. Men, H.; Fan, Z. Atomic ordering in liquid aluminium induced by substrates with misfits. *Comput. Mater. Sci.* **2014**, *85*, 1–7. [CrossRef]
63. Hashibon, A.; Adler, J.; Finnis, M.W.; Kaplan, W.D. Ordering at solid-liquid interfaces between dissimilar materials. *Interface Sci.* **2001**, *9*, 175–181. [CrossRef]
64. Hashibon, A.; Adler, J.; Finnis, M.W.; Kaplan, W.D. Atomistic study of structural correlations at a liquid-solid interface. *Comput. Mater. Sci.* **2002**, *24*, 443–452. [CrossRef]
65. Gibbs, J.W. *The Collected Works of J. Willard Gibbs*; Yale University Press: New Haven, CT, USA, 1948.
66. Seah, M.P. Interface adsorption, embrittlement and fracture in metallurgy: A review. *Surf. Sci.* **1975**, *53*, 168–212. [CrossRef]
67. Kaplan, W.D.; Chatain, D.; Wynblatt, P.; Carter, W.C. A review of wetting versus adsorption, complexions, and related phenomena: The rosetta stone of wetting. *J. Mater. Sci.* **2013**, *48*, 5681–5717. [CrossRef]
68. Kim, W.T.; Cantor, B. An adsorption model of the heterogeneous nucleation of solidification. *Acta Metall. Mater.* **1994**, *42*, 3115–3127. [CrossRef]
69. Han, Y.; Dai, Y.; Shu, D.; Wang, J.; Sun, B. First-principles calculations on the stability of Al/TiB_2 interface. *Appl. Phys. Lett.* **2006**, *89*, 144107. [CrossRef]
70. Qin, T.; Fan, Z. Reconstruction of 2D Al_3Ti on TiB_2 in an aluminium melt. *IOP Conf. Ser. Mater. Sci. Eng.* **2012**, *27*, 012004. [CrossRef]
71. Wang, Y.; Que, Z.P.; Hashimoto, T.; Zhou, X.; Fan, Z. Mechanism for Si poisoning of Al-Ti-B grain refiners in Al alloys. *Metall. Mater. Trans. A* **2020**, *51*, 5743–5757. [CrossRef]
72. Li, H.T.; Wang, Y.; Fan, Z. Mechanisms of enhanced heterogeneous nucleation during solidification in binary Al-Mg-alloys. *Acta Mater.* **2012**, *60*, 1528–1537. [CrossRef]
73. Jiang, B.; Liu, W.; Qiu, D.; Zhang, M.X.; Pan, F. Grain refinement of Ca addition in a twin-roll-cast Mg-3Al-1Zn alloy. *Mater. Chem. Phys.* **2012**, *133*, 611–616. [CrossRef]
74. Wang, F.; Liu, Z.; Qiu, D.; Taylor, J.A.; Easton, M.A.; Zhang, M.X. Revisiting the role of peritectics in grain refinement of Al-alloys. *Acta Mater.* **2013**, *61*, 360–370. [CrossRef]
75. Wang, F.; Qiu, D.; Liu, Z.; Taylor, J.A.; Easton, M.A.; Zhang, M.X. The grain refining mechanism of cast Al by zirconium. *Acta Mater.* **2013**, *61*, 5636–5645. [CrossRef]
76. Peng, G.S.; Wang, Y.; Fan, Z. Competitive heterogeneous nucleation between Zr and MgO particles in commercial purity magnesium. *Metall. Mater. Trans. A* **2018**, *49*, 2182–2192. [CrossRef]
77. Gao., F.; Fan, Z. Competition for nucleation and grain initiation during solidification. *Metals* **2022**. *in progress*.
78. Gao, F.; Fan, Z. Effect of nucleant particle agglomeration on grain size. *Metall. Mater. Trans. A* **2022**, *53*, 810–822. [CrossRef]
79. Hodaj, F.; Durand, F. Equiaxed grains in multicomponent alloys: Effect of growth rate. *Acta Mater.* **1997**, *45*, 2121–2127. [CrossRef]
80. Fan, Z.; Gao, F.; Zhou, L.; Lu, S.Z. A new concept of growth restriction. *Acta Mater.* **2018**, *152*, 248–257. [CrossRef]
81. Aaron, H.B.; Fainstein, D.; Kotler, G.R. Diffusion-limited phase transformations: A comparison and critical evaluation of the mathematical approximations. *J. Appl. Phys.* **1970**, *41*, 4404–4410. [CrossRef]
82. Zener, C. Theory of growth of spherical precipitates from solid solution. *J. Appl. Phys.* **1949**, *20*, 950–953. [CrossRef]
83. Available online: https://computherm.com/databases (accessed on 8 August 2022).
84. The Al Association. *Standard Test Procedure for Al Alloy Grain Refiners (TP-1)*; The Al Association: Washington, DC, USA, 1990.
85. Hunt, J. Steady state columnar and equiaxed growth of dendrites and eutectic. *Mater. Sci. Eng.* **1984**, *65*, 75–83. [CrossRef]
86. Zhou, L.; Gao, F.; Peng, G.S.; Alba-Baena, N. Effect of potent TiB_2 addition levels and impurities on the grain refinement of Al. *J. Alloys Comp.* **2016**, *689*, 401–407. [CrossRef]

87. Zhou, L. The Role of Various Solutes on Grain Refinement of Aluminum Alloys with Al-Ti-B Inoculations. Ph.D. Thesis, Brunel University, London, UK, 2015.
88. Fan, Z.; Wang, Y.; Xia, M.; Arumuganathar, S. Enhanced heterogeneous nucleation in AZ91D alloy by intensive melt shearing. *Acta Mater.* **2009**, *57*, 4891–4901. [CrossRef]
89. Fan, Z.; Jiang, B.; Zuo, Y. Apparatus and Method for Liquid Metals Treatment. U.S. Patent US 9.498,820 B2, 22 November 2016.
90. Fan, Z.; Zuo, Y.; Jiang, B. A new technology for treating liquid metals with intensive melt shearing. *Mater. Sci. Forum* **2010**, *690*, 141–144.
91. Patel, J.B.; Yang, X.; Mendis, C.L.; Fan, Z. Melt conditioning of light metals by application of high shear for improved microstructure and defect control. *JOM* **2017**, *69*, 1071–1076. [CrossRef]
92. Men, H.; Jiang, B.; Fan, Z. Mechanisms of grain refinement by intensive shearing of AZ91alloy melt. *Acta Mater.* **2010**, *58*, 6526–6534. [CrossRef]
93. Wang, S.; Wang, Y.; Ramasse, Q.; Fan, Z. The nature of native MgO in Mg and its alloys. *Metall. Mater. Trans. A* **2020**, *51*, 2957–2974. [CrossRef]
94. Peng, G.S.; Gu, Y.C.; Song, G.S.; Wang, Y.; Chen, S.Y. New insight of Ca element refining grain structure in commercial purity Mg based on the first-principle calculation. *Int. J. Cast Met. Res.* **2021**, *34*, 6–13. [CrossRef]
95. Wang, S.H.; Wang, F.; Wang, Y.; Ramasse, Q.M.; Fan, Z. Segregation of Ca at the Mg/MgO interface and its effect on grain refinement of Mg alloys. *IOP Conf. Ser. Mater. Sci. Eng.* **2019**, *529*, 012048. [CrossRef]
96. Wang, S.H. Characterisation of Native MgO and Its Roles in Solidification of Mg Alloys. Ph.D. Thesis, Brunel University, London, UK, 2020.